

Supporting Information

Wintertime Optical Properties of Primary and Secondary Brown Carbon at a Regional Site in the North China Plain

Qiyuan Wang,^{,†,‡} Jianhuai Ye,[§] Yichen Wang,[¶] Ting Zhang,^{†,‡} Weikang Ran,[†] Yunfei Wu,[#] Jie Tian,^{†,‡} Li Li,[†] Yaqing Zhou,[†] Steven Sai Hang Ho,[∇] Bo Dang,[◇] Qian Zhang,[⊥] Renjian Zhang,[#] Yang Chen,[○] Chongshu Zhu,^{†,‡} and Junji Cao^{*,†,‡}*

[†]Key Laboratory of Aerosol Chemistry and Physics, State Key Laboratory of Loess and Quaternary Geology, Institute of Earth Environment, Chinese Academy of Sciences, Xi'an 710061, China

[‡]CAS Center for Excellence in Quaternary Science and Global Change, Xi'an 710061, China

[§]School of Engineering and Applied Sciences, Harvard University, Cambridge, Massachusetts 02138, USA

[¶]School of Humanities, Economics and Law, Northwestern Polytechnical University, Xi'an 710129, China

[#]Key Laboratory of Regional Climate-Environment Research for Temperate East Asia, Institute of Atmospheric Physics, Chinese Academy of Sciences, Beijing 100029, China

[∇]Division of Atmospheric Sciences, Desert Research Institute, Reno, Nevada 89512, USA

[⊥]Shannxi Key Laboratory of Measurement and Control Technology for Oil and Gas Wells,
Xi'an Shiyou University, Xi'an 710065, China

[◇]Key Laboratory of Northwest Resource, Environment and Ecology, MOE, Xi'an University
of Architecture and Technology, Xi'an 710055, China

[°]Chongqing Institute of Green and Intelligent Technology, Chinese Academy of Sciences,
Chongqing 400714, China

*Corresponding Author

E-mail: wangqy@ieecas.cn; Phone: +86-29-62336273

E-mail: cao@loess.llqg.ac.cn; Phone: +86-29-62336205

■ Contents of this file

Text S1 to S6

Tables S1 to S3

Figures S1 to S15

■ Text S1. Correction of Aethalometer™ Absorption

Filter-based light absorption techniques suffer from shadowing and filter matrix scattering artifacts.¹ The seven-wavelength Aethalometer™ (Model AE33, Magee Scientific, Berkeley, CA, USA) applies a two-parallel spot measurement technology to avoid the shadowing effect, and a manufacturer default factor (known as the “*C*-value”) of 1.57 can be used to compensate for the matrix scattering effects caused by tetrafluoroethylene (TFE)-coated glass filters (Pallflex “Fiber-film” T60A20).² However, the *C*-value is not constant, and therefore, a photoacoustic extinctionsmeter (PAX) operating at $\lambda = 532$ nm was installed in parallel with the AE33 to derive a site-specific *C*-value. The PAX measures light scattering and absorption coefficients simultaneously using a built-in wide-angle-integrating reciprocal nephelometer and a photoacoustic device, respectively. Ammonium sulfate particles were used to calibrate light scattering for the PAX and fullerene soot for the absorption coefficients. More detailed information regarding the PAX calibration procedures may be found in Wang et al.³ A scatter plot of AE33 versus PAX absorption coefficients is shown in Figure S1. The AE33 absorption coefficient was higher than the PAX absorption by a factor of 2.6, which is comparable to values found in previous studies (1.2–2.1).^{4–6} Therefore, the *C*-value of 4.1 ($= 2.6 \times 1.57$) was used for correcting the filter matrix scatterings effect of the Aethalometer™ absorption in this study. It should be noted that *C*-values may be dependent upon wavelength and chemical-composition,⁷ and our single correction factor may underestimate the light absorption coefficients at $\lambda = 370$ and 470 nm but overestimate those at $\lambda = 590$ and 660 nm.

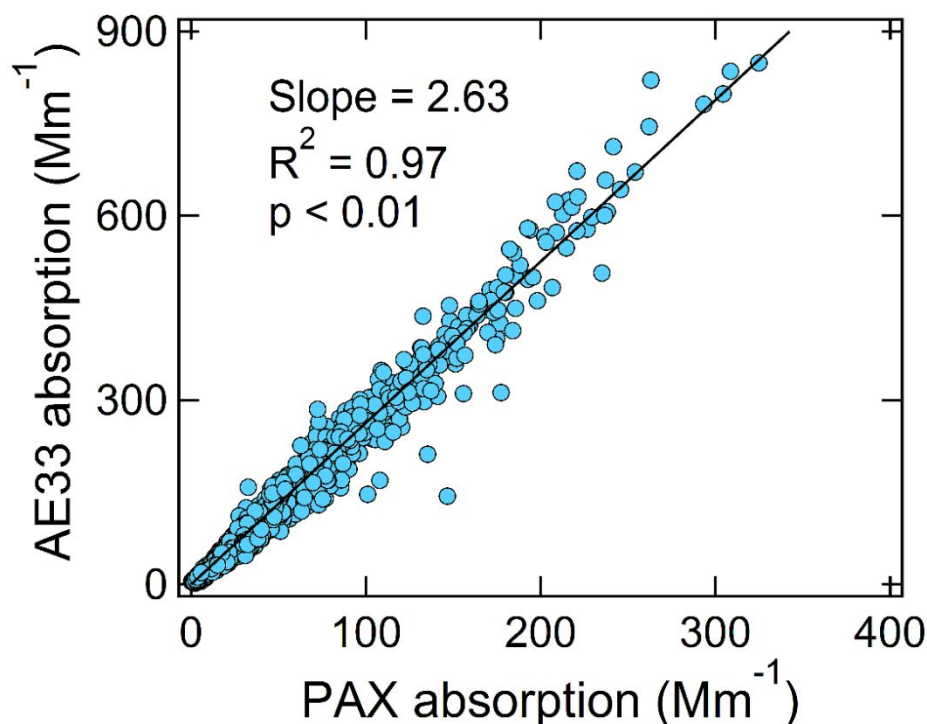


Figure S1. Scatter plot showing the relationship between aerosol light absorption measured by seven-wavelength Aethalometer™ (Model AE33) and photoacoustic extinctions (PAX).

■ Text S2. Source Apportionment of Organic Aerosol (OA)

The mass spectra detected by the quadruple aerosol chemical speciation monitor (Q-ACSM) were analyzed using the Multilinear Engine (ME-2) algorithm⁸ implemented with the toolkit SoFi (Source Finder)⁹ to resolve the OA sources. Detailed information on the ME-2 analyses is given elsewhere.⁹⁻¹¹ Briefly, a solution was first obtained by unconstrained positive matrix factorization (PMF)¹² to determine the potential numbers and types of factors. Subsequently, mass spectra that were obtained from previous field or laboratory measurements are introduced as reference spectra to constrain one or more of the solution spectra. This constraint is achieved by setting *a*-values over a range from 0 to 1 in the ME-2 solver. The *a*-values represent the extent to which the reference profiles are allowed to vary; for example, 0.1 represents a

maximum of $\pm 10\%$ variability of each m/z signal. To eliminate the influences of the naphthalene internal standard signal at m/z 127–129 and the low signal-to-noise (S/N) ratios of larger ions, only $m/z < 120$ were considered in this study. The organic and the organic error matrices used as inputs were automatically derived from the Q-ACSM data analysis software. Data points with a low S/N (< 0.2) were discarded, and those with S/N from 0.2–2 were down-weighted by a factor of 2. The unconstrained PMF runs showed that the most physically interpretable profiles were found with a four-factor solution, i.e., hydrocarbon-like OA (HOA), biomass burning OA (BBOA), coal combustion OA (CCOA), and oxygenated OA (OOA). However, mixing was obvious in the mass spectra for BBOA and CCOA, and to account for this, reference profiles of BBOA and CCOA obtained from winter Beijing¹⁰ were introduced to constrain these two factors by varying the α -value from 0 to 0.5 (with a 0.1 step). The other factors were left free. The final mass spectral profiles and time series of the mass concentrations of the four OA factors are shown in Figure S2.

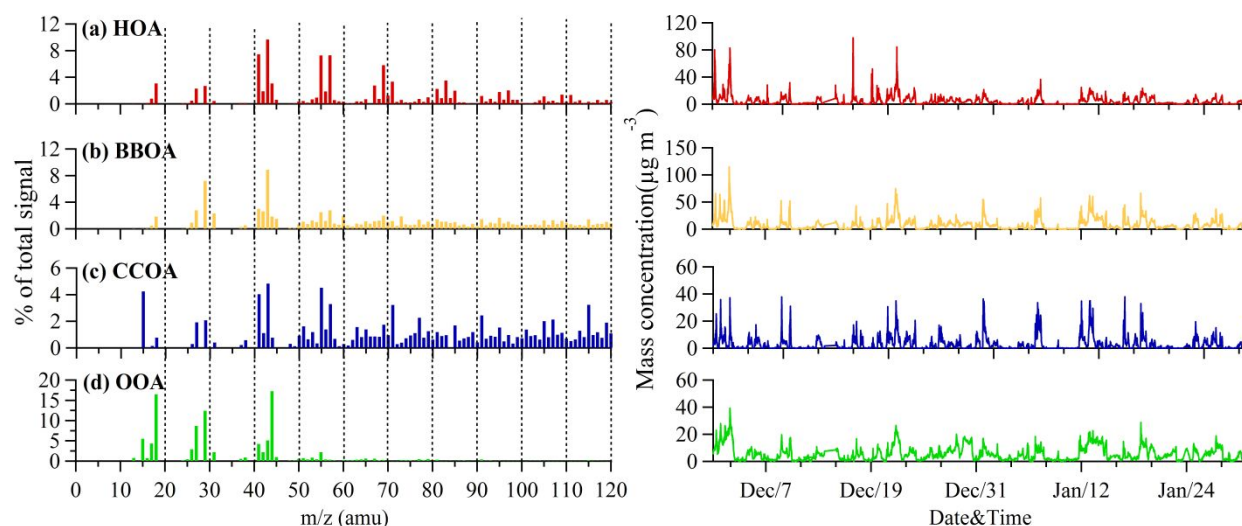


Figure S2. (left panel) Mass spectra of hydrocarbon-like OA (HOA), biomass burning OA (BBOA), coal combustion OA (CCOA), and oxygenated OA (OOA); and (right panel) the corresponding time series of mass concentrations for the OA factors.

■ Text S3. Calculation of Black Carbon (BC) Mass Concentrations

Daily PM₁ quartz-fiber filters (QM/A; Oregon, USA) were collected simultaneously with the AE33 Aethalometer™ measurements from 09:00 local time to 09:00 the next day using a mini-volume air sampler (Airmetrics, Oregon, USA) at a flow rate of 5 L min⁻¹. Elemental carbon (EC) collected on each filter was analyzed by a Desert Research Institute (DRI) Model 2001 thermal/optical carbon analyzer (Atmoslytic Inc., Calabasa, CA, USA).¹³ A default BC mass absorption cross section (MAC_{BC} , m² g⁻¹) can be used for the AE33 to obtain the BC loadings; however, the MAC_{BC} is site-dependent because of the variability in BC particle size, morphology, and mixing state.^{14,15} Therefore, daily EC loadings were used to obtain a representative MAC_{BC} for Xianghe. As shown in Figure S3, daily aerosol light absorption measured by AE33 at $\lambda = 880$ nm ($Abs(880)$) showed a strong correlation ($R^2 = 0.87$, $p < 0.01$) with EC mass concentrations. The slope of 4.8 m² g⁻¹ is comparable with the results of a study of Yang et al. at Xianghe during the springtime (5.9 m² g⁻¹),¹⁶ and that value was in this study used to retrieve the mass concentrations of BC.

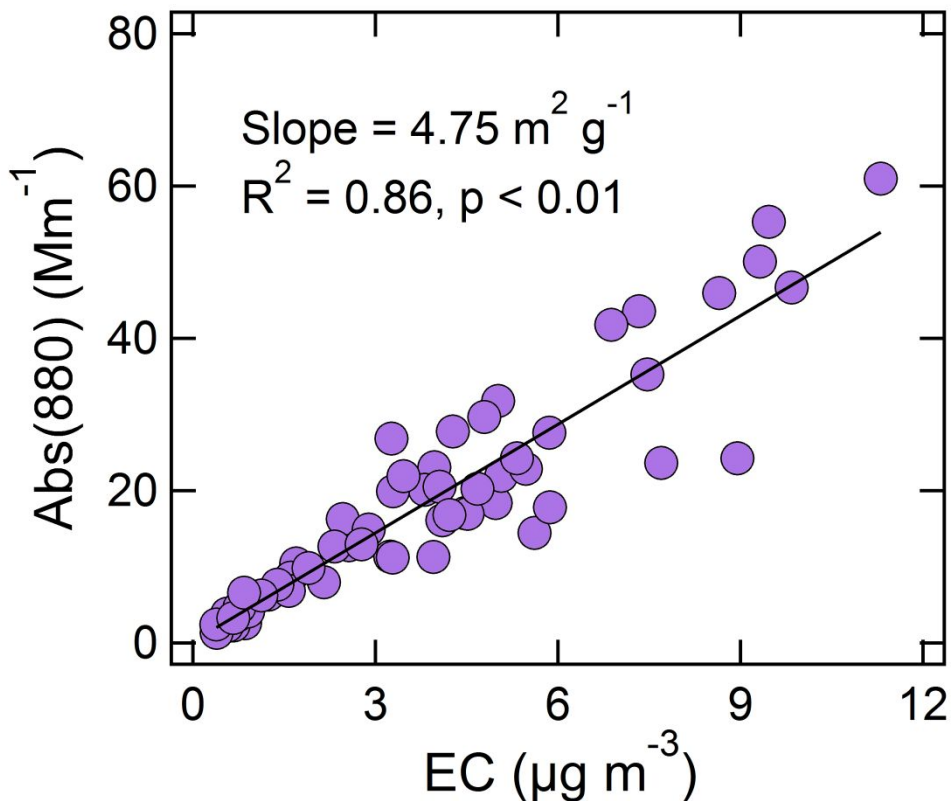


Figure S3. Scatter plot of aerosol light absorption at wavelength of 880 nm ($Abs(880)$) versus elemental carbon (EC) mass concentrations during the campaign.

■ **Text S4. Calculation of Brown Carbon (BrC) Absorption**

The wavelength dependence of aerosol light absorption ($Abs(\lambda)$) can be characterized by the absorption Ångström exponent (AAE):¹⁷

$$Abs(\lambda) = K \times \lambda^{-AAE} \quad (S1)$$

where K is a constant related to the aerosol mass concentration. Previous studies have suggested that $AAE = 1$ indicates the dominance of BC aerosol while $AAE > 1$ suggests the presence of non-BC materials, such as BrC aerosol.¹⁷

Here, we assumed a negligible absorption by dust during the campaign, and thus, $Abs(\lambda)$ can be divided into BC and BrC absorption:

$$Abs(\lambda) = Abs_{BrC}(\lambda) + Abs_{BC}(\lambda) \quad (S2)$$

where $Abs_{BrC}(\lambda)$ is the absorption caused by BrC at $\lambda = 370, 470, 520, 590,$ or 660 nm while $Abs_{BC}(\lambda)$ is the absorption contributed by BC at the same wavelength. To determine $Abs_{BC}(\lambda)$ at each wavelength, we assumed that BC was the only absorber at $\lambda = 880$ nm, and thus the $Abs_{BC}(\lambda)$ ($\lambda = 370, 470, 520, 590,$ and 660) can be extrapolated from the following formula:¹⁸

$$Abs_{BC}(\lambda) = Abs(880) \times \left(\frac{\lambda}{880}\right)^{-AAE_{BC}} \quad (S3)$$

where AAE_{BC} represents BC spectral dependence, and the value of 1.1 was used based on previous studies.¹⁹ Finally, one can obtain the $Abs_{BrC}(\lambda)$ as follows:

$$Abs_{BrC}(\lambda) = Abs(\lambda) - Abs(880) \times \left(\frac{\lambda}{880}\right)^{-AAE_{BC}} \quad (S4)$$

■ Text S5. Assessment of a Multiple Linear Regression (MLR) Model

The index of agreement (IOA) was used to evaluate the performance of the MLR method. The IOA varies from 0 to 1, and it describes the relative difference between the predicted and measured values, with a value of 1 indicating perfect performance of the MLR prediction. These parameters were calculated as follows:²⁰

$$IOA = 1 - \frac{\sum_{i=1}^N (P_i - O_i)^2}{\sum_{i=1}^N (|P_i - P_{ave}| + |O_i - O_{ave}|)^2} \quad (S5)$$

where P_i and P_{ave} represent each predicted light absorption coefficient and the average value, respectively; O_i and O_{ave} are the observed light absorption coefficient and the average value, respectively; and N represents the total number of predictions used for comparison.

■ Text S6. Calculation of Aerosol Liquid Water Content (ALWC)

The aerosol liquid water content (ALWC) was estimated using the Extended AIM Aerosol Thermodynamics Model (E-AIM) (Model III and Model IV).^{21,22} Hourly-average concentrations of major ions NH_4^+ , SO_4^{2-} , NO_3^- , and Cl^- were input parameters, and they were obtained from the Q-ACSM measurements. The concentrations of H^+ were calculated from charge balance. Relative humidity and temperature were obtained from an automatic weather station installed at the Xianghe Atmospheric Integrated Observatory. The contributions of organic compounds were not included in the calculations.

Table S1. Correlation matrix for primary brown carbon absorption ($Abs_{BrC,pri}(\lambda)$) for different wavelengths (370, 470, 520, 590, and 660 nm) during the campaign.

	$Abs_{BrC,pri}(370)$	$Abs_{BrC,pri}(470)$	$Abs_{BrC,pri}(520)$	$Abs_{BrC,pri}(590)$	$Abs_{BrC,pri}(660)$
$Abs_{BrC,pri}(370)$	1.00				
$Abs_{BrC,pri}(470)$	0.99	1.00			
$Abs_{BrC,pri}(520)$	0.94	0.95	1.00		
$Abs_{BrC,pri}(590)$	0.95	0.98	0.97	1.00	
$Abs_{BrC,pri}(660)$	0.80	0.82	0.94	0.88	1.00

Table S2. Correlation matrix for secondary brown carbon absorption ($Abs_{BrC,sec}(\lambda)$) for different wavelengths (370, 470, 520, 590, and 660 nm) during the campaign.

	$Abs_{BrC,sec}(370)$	$Abs_{BrC,sec}(470)$	$Abs_{BrC,sec}(520)$	$Abs_{BrC,sec}(590)$	$Abs_{BrC,sec}(660)$
$Abs_{BrC,sec}(370)$	1.00				
$Abs_{BrC,sec}(470)$	0.81	1.00			
$Abs_{BrC,sec}(520)$	0.87	0.79	1.00		
$Abs_{BrC,sec}(590)$	0.78	0.73	0.88	1.00	
$Abs_{BrC,sec}(660)$	0.78	0.58	0.97	0.86	1.00

Table S3. Summary of the multiple linear regression results based on the 60% of the data from the first part of the campaign (1 December 2017 to 6 January 2018).

Parameter ^a	Mean ^b	Standard deviation	p value
MAC _{BBOA} (370)	3.35	0.16	< 0.001
MAC _{CCOA} (370)	5.73	0.32	< 0.001
MAC _{HOA} (370)	0.52	0.16	0.001

^aMAC_{BBOA}(370), MAC_{CCOA}(370), and MAC_{HOA}(370) represent the mass absorption cross sections for biomass burning organic aerosol (OA), coal combustion OA, and hydrocarbon-like OA at $\lambda = 370$ nm, respectively.

^bunits for MAC are m² g⁻¹.

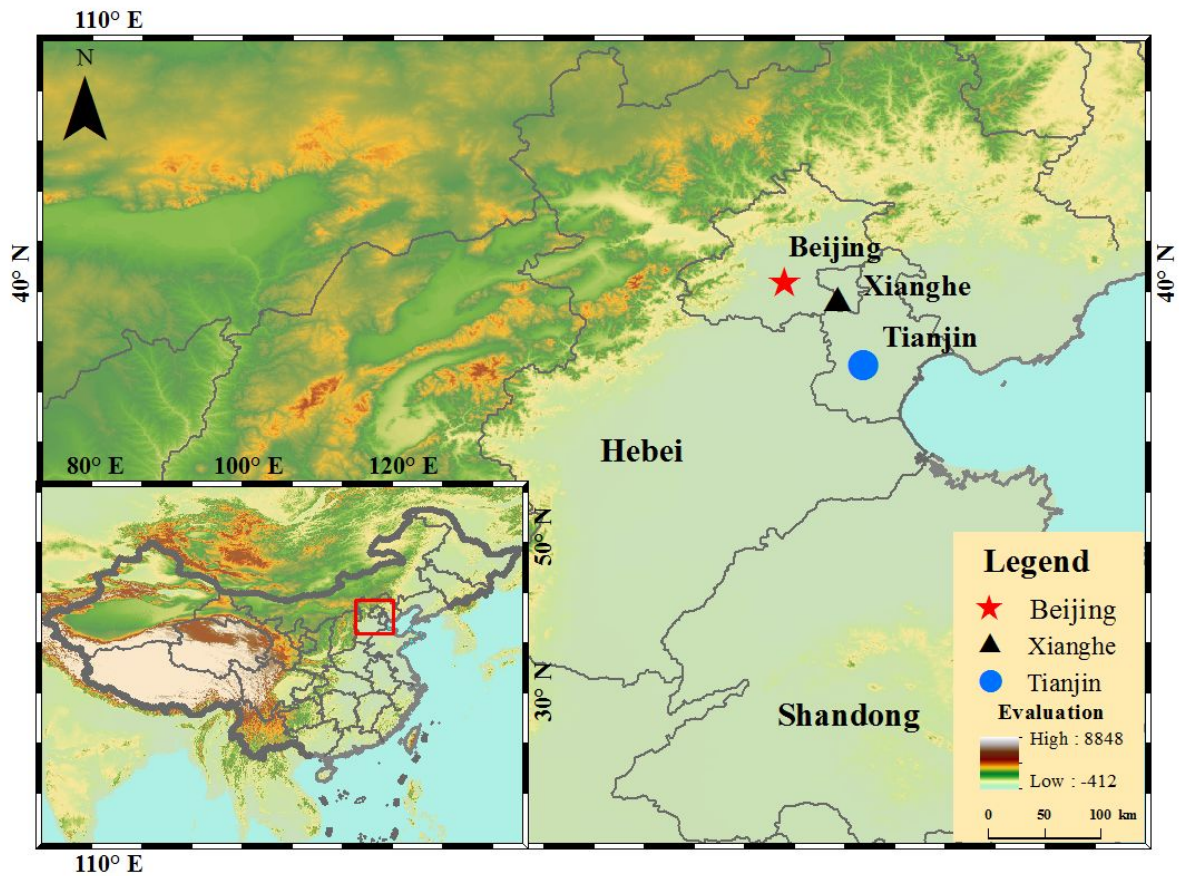


Figure S4. Map showing the Xianghe sampling site and surrounding areas. The map was drawn using ArcGIS software, and the base map is the World Topographic Map from ESRI® (<http://www.arcgis.com/home/item.html?id=30e5fe3149c34df1ba922e6f5bbf808f>).

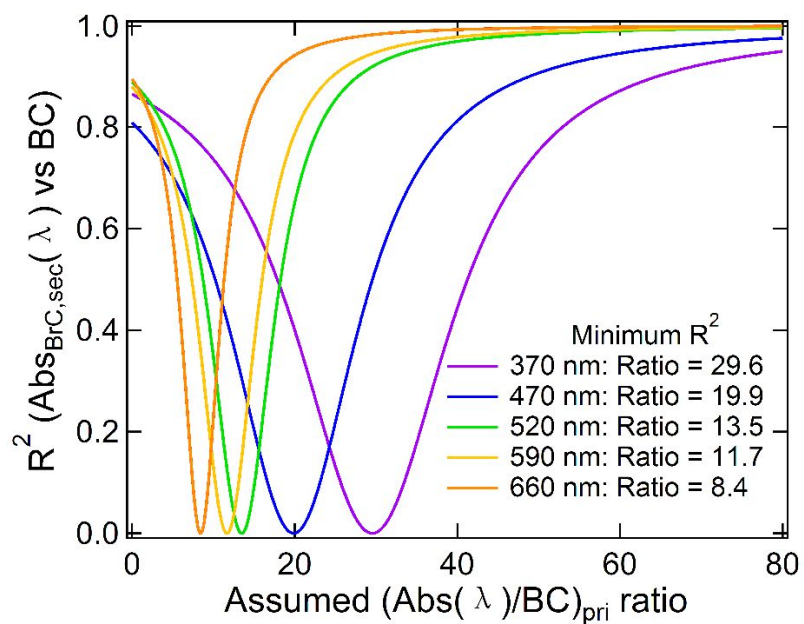


Figure S5. Coefficients of determination (R^2) for secondary brown carbon absorption ($Abs_{BrC,sec}(\lambda)$) at $\lambda = 370, 470, 520, 590,$ and 660 nm versus black carbon (BC) mass concentration plotted against assumed ratios for light absorption to BC in primary emissions ($Abs(\lambda)/BC)_{pri}$).

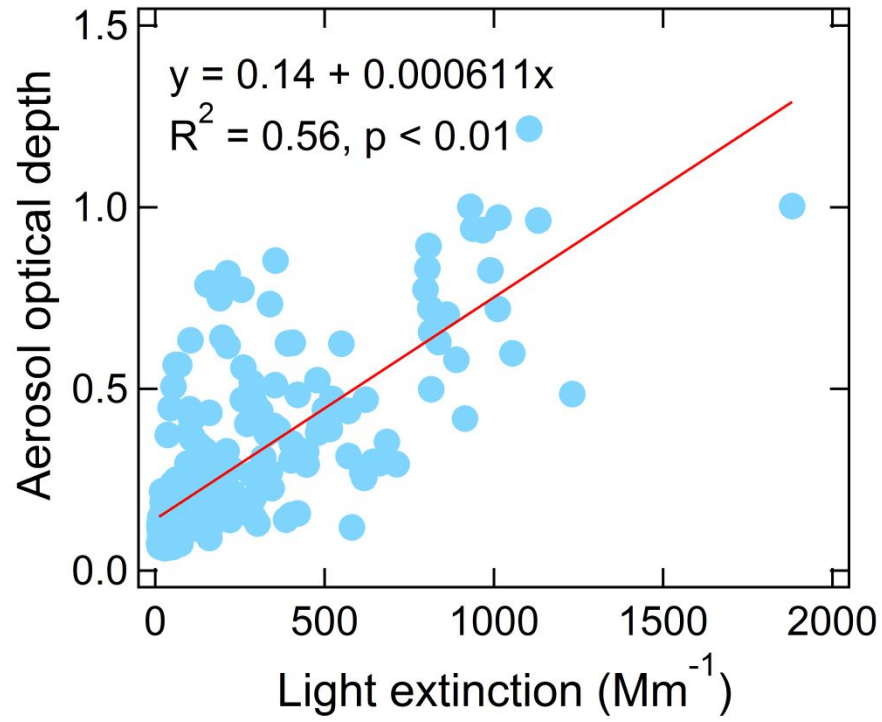


Figure S6. Scatter plot of aerosol optical depth at $\lambda = 500$ nm measured with a sun photometer versus aerosol light extinction coefficient at $\lambda = 532$ nm measured with a photoacoustic extinctionsimeter.

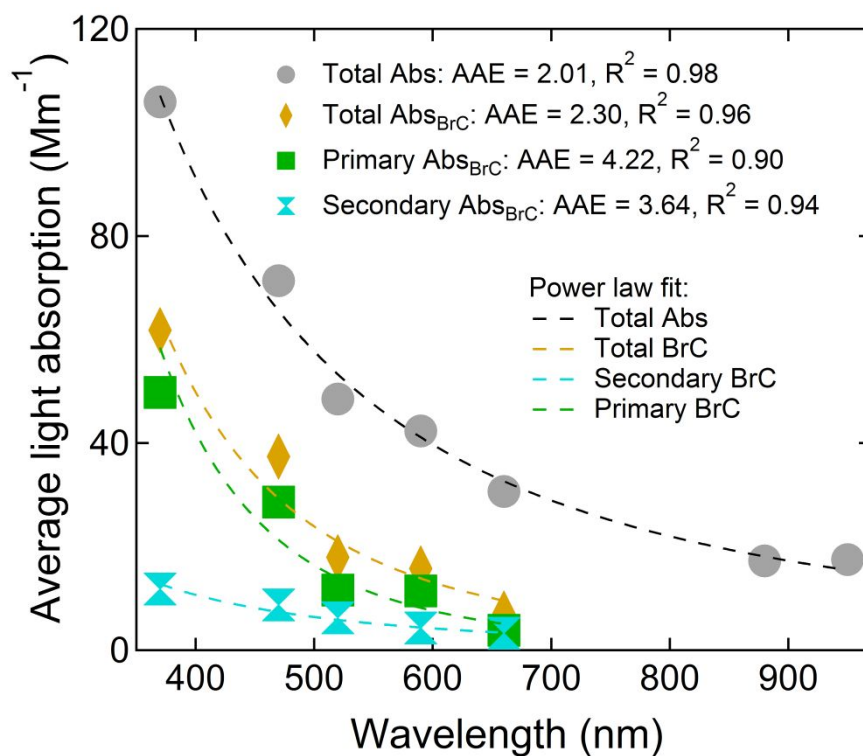


Figure S7. Light absorption (Abs) at specific wavelengths contributed by total aerosol, total brown carbon (BrC) (Abs_{BrC}), as well as primary and secondary BrC . Each data point represents the Abs averaged over the entire campaign. AAE stands for Absorption Ångström exponent.

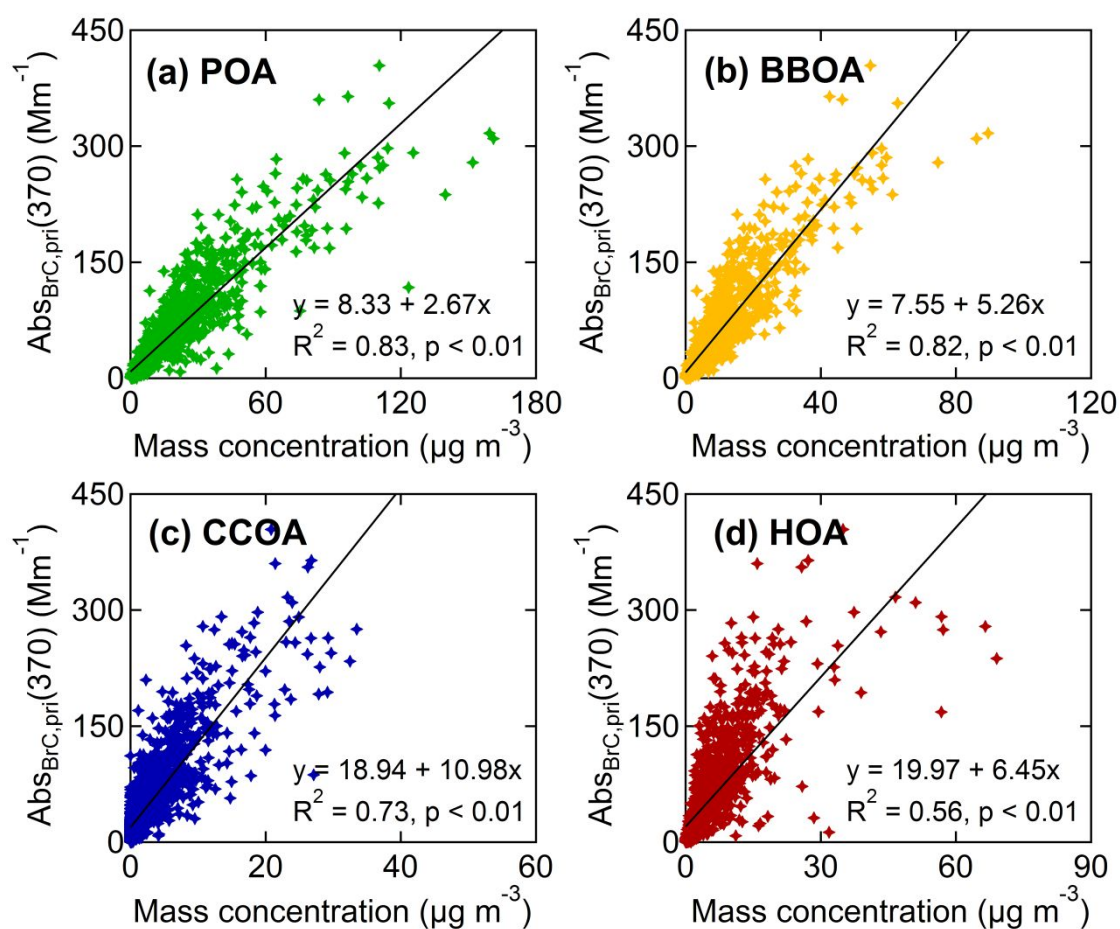


Figure S8. Scatter plots of primary brown carbon absorption at $\lambda = 370$ nm ($Abs_{BrC,pri}(370)$) versus the mass concentrations of (a) primary organic aerosol (POA) and its sub-types (b) biomass burning organic aerosol (BBOA), (c) coal combustion organic aerosol (CCOA), and (d) hydrocarbon-like organic aerosol (HOA) during the campaign.

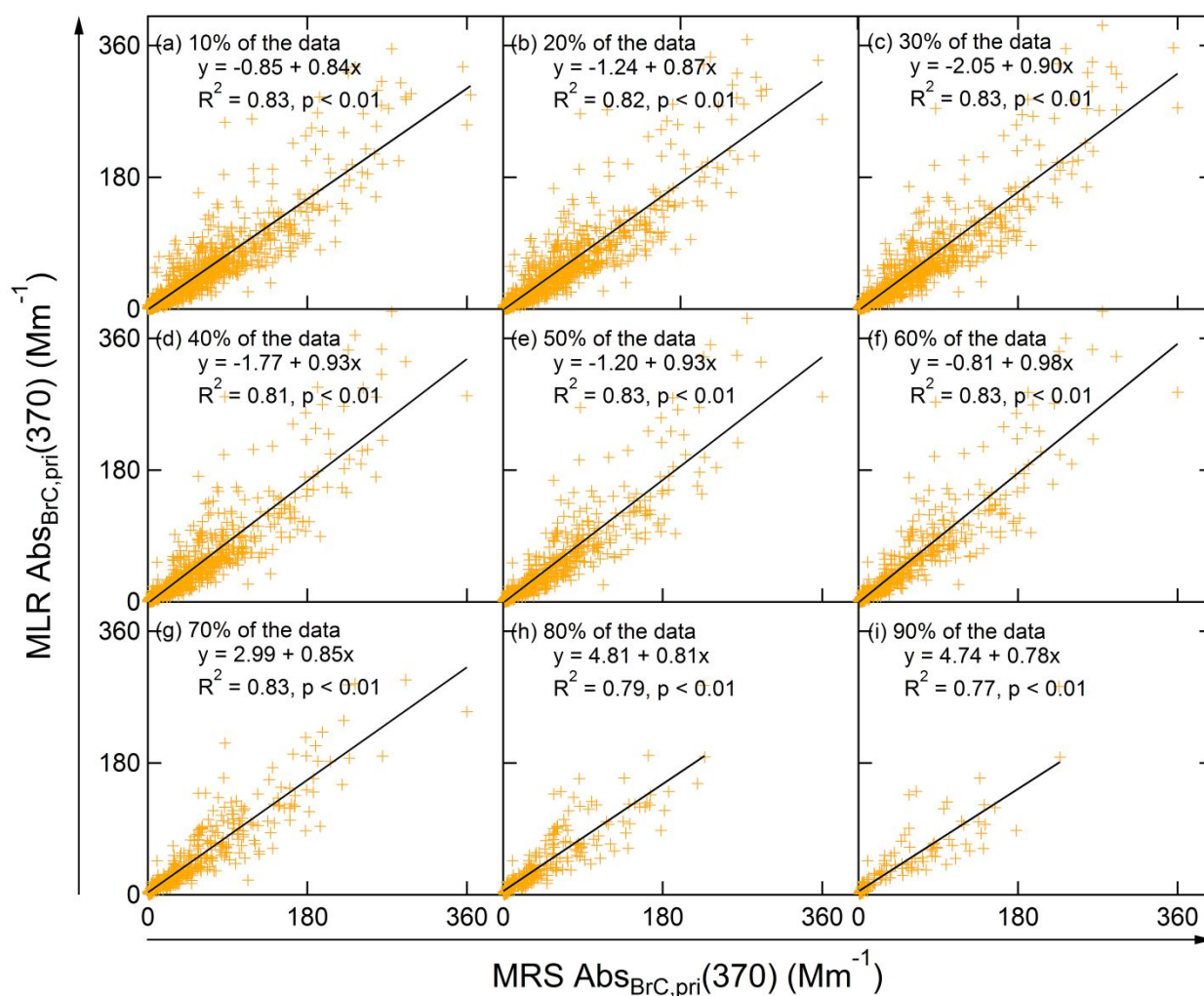
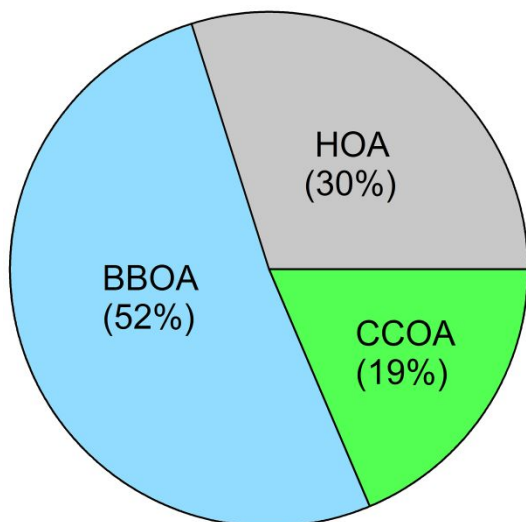


Figure S9. Scatter plots of primary brown carbon absorption at $\lambda = 370$ nm ($Abs_{BrC,pri}(370)$) obtained from a multiple linear regression (MLR) method versus matching values estimated by a minimum R -squared (MRS) approach: panels (a)–(i) show the results when 10%, 20%, 30%, 40%, 50%, 60%, 70%, 80%, and 90% of total data were first utilized to establish the MLR function, and the rest data (90%, 80%, 70%, 60%, 50%, 40%, 30%, 20%, and 10%) were used to test and verify the results.

(a) Primary organic aerosol



(b) Primary BrC absorption

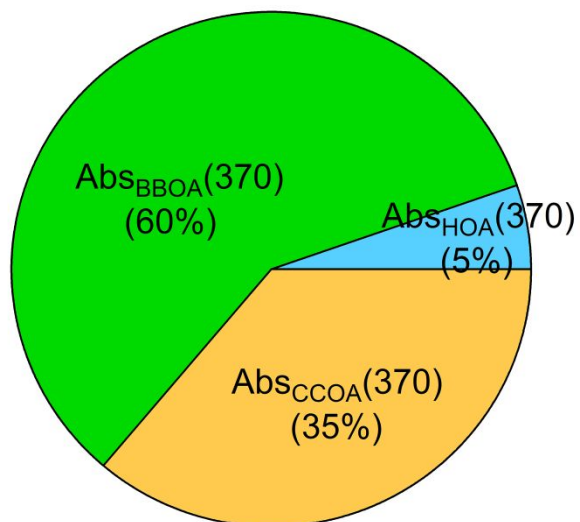


Figure S10. Contributions of biomass burning organic aerosol (BBOA), coal combustion organic aerosol (CCOA), and hydrocarbon-like organic aerosol (HOA) to (a) mass concentration of primary organic aerosol and (b) primary brown carbon absorption at $\lambda = 370$ nm during the campaign. $Abs_{BBOA}(370)$, $Abs_{CCOA}(370)$, and $Abs_{HOA}(370)$ represent the light absorption contributed by BBOA, CCOA, and HOA, respectively.

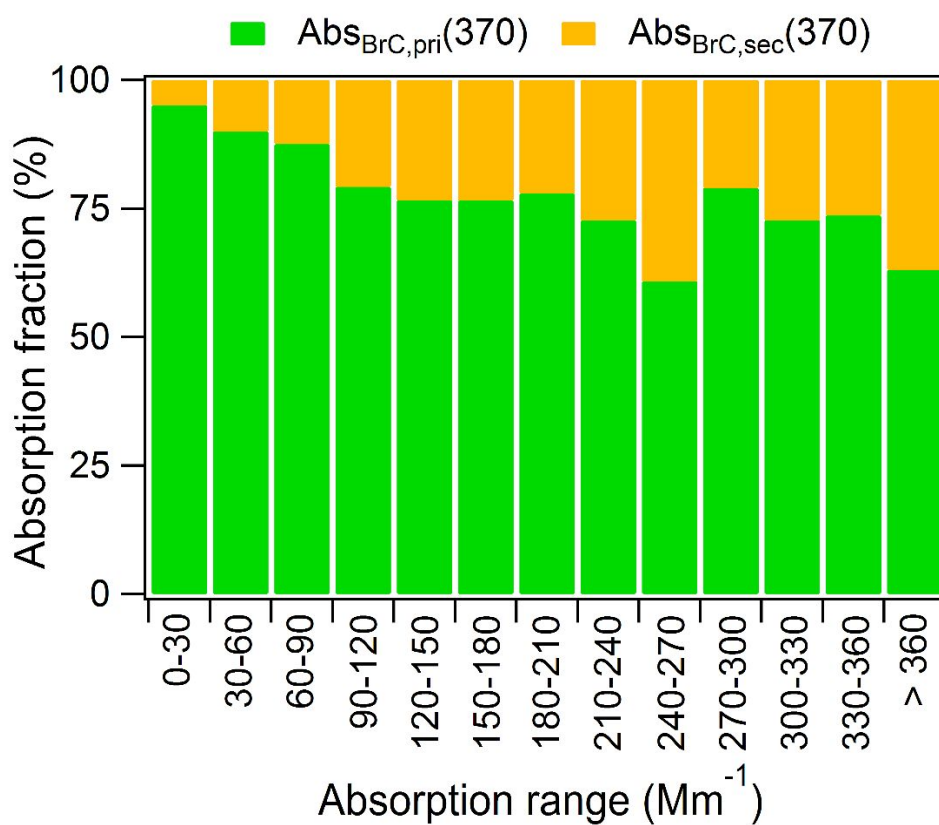


Figure S11. Variations of the fraction of absorption at $\lambda = 370$ nm contributed by primary and secondary brown carbon ($Abs_{\text{BrC, pri}}(370)$ and $Abs_{\text{BrC, sec}}(370)$, respectively) for different absorption ranges during the campaign.

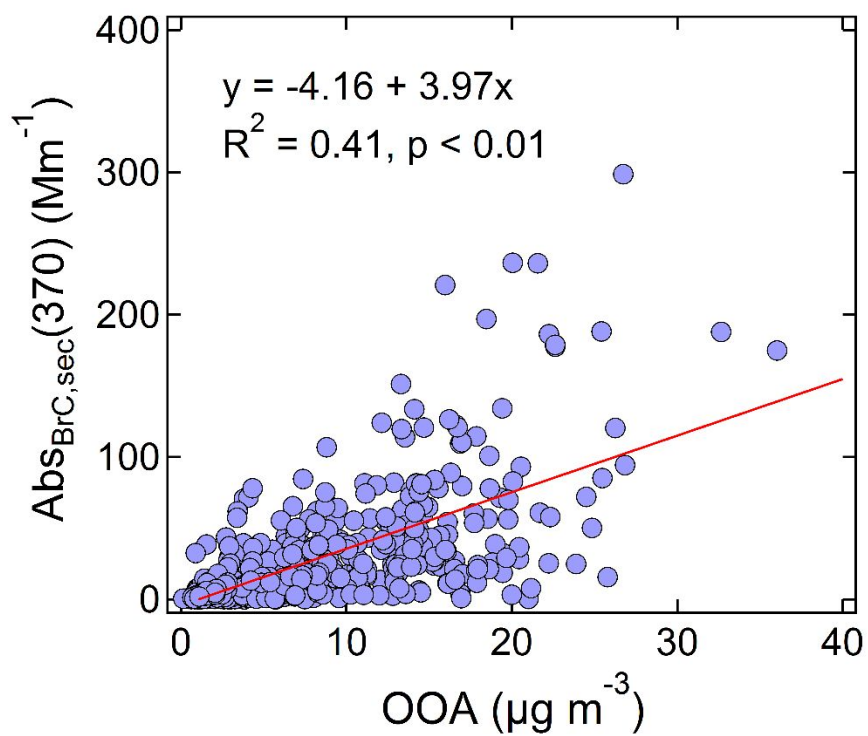


Figure S12. Relationship between light absorption at $\lambda = 370$ nm contributed by secondary brown carbon ($Abs_{BrC,sec}(370)$) and oxygenated organic aerosol (OOA) mass concentrations.

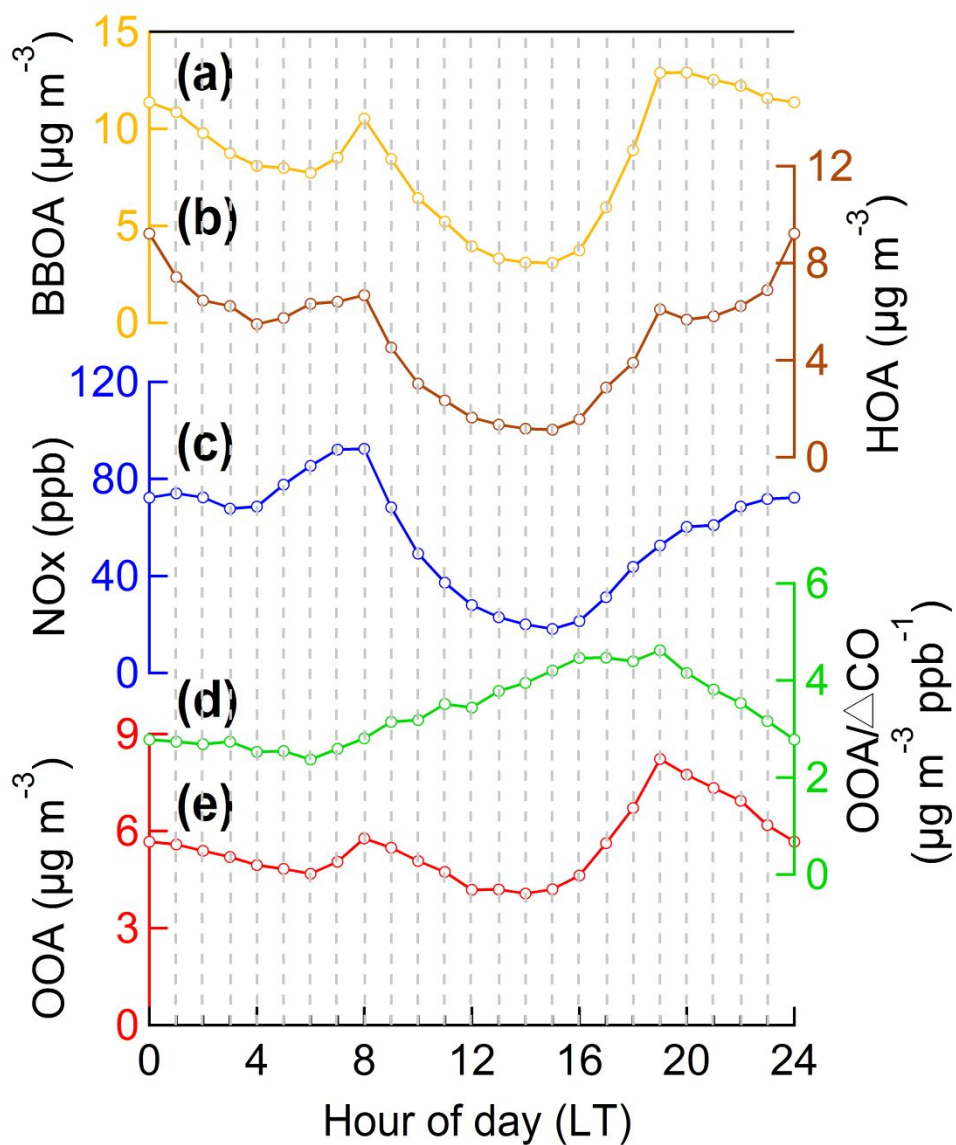


Figure S13. Diurnal variations in the concentrations of hydrocarbon-like organic aerosol (HOA), biomass burning organic aerosol (BBOA), oxygenated organic aerosol (OOA), and nitrogen oxide (NO_x) as well as the ratio of OOA/(background-corrected CO, ΔCO). LT stands for local time.

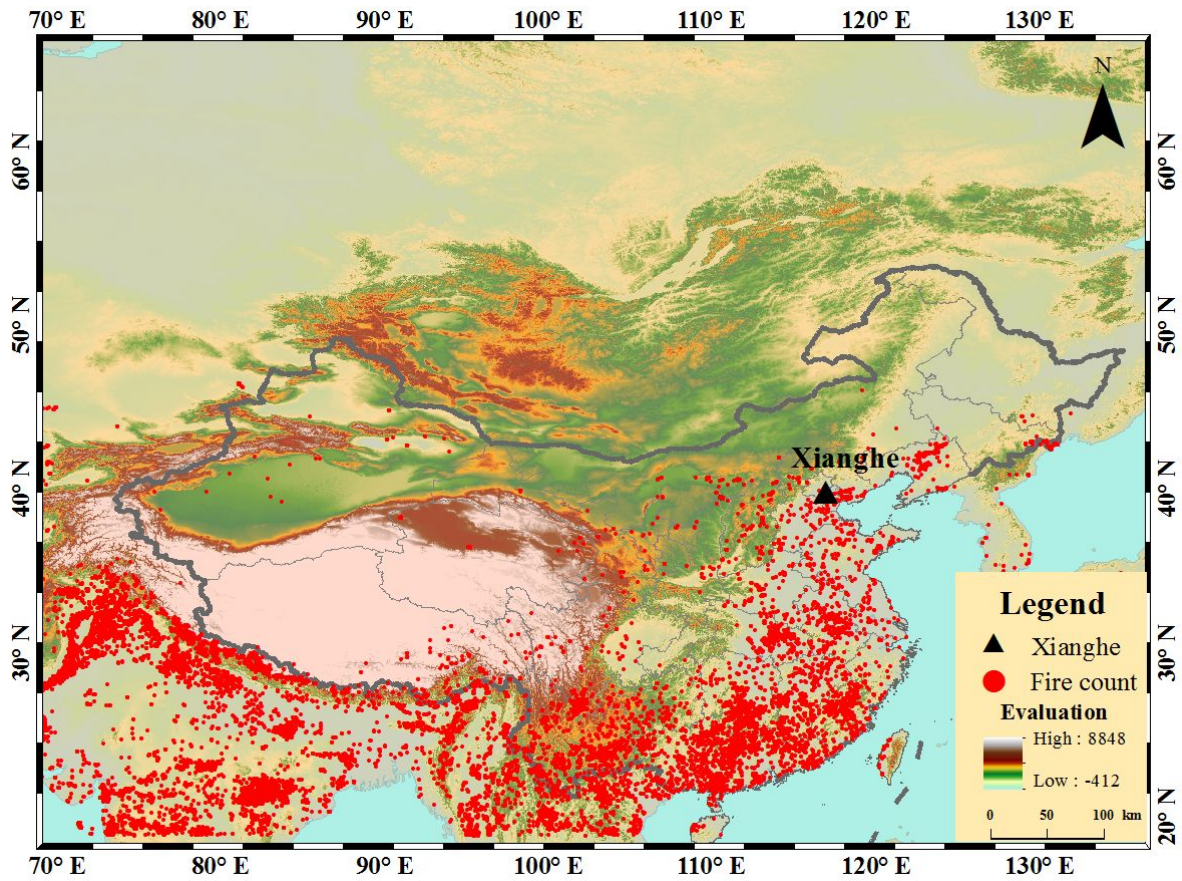


Figure S14. Fire counts in China during the campaign. The map was drawn using ArcGIS software, and the base map is the World Topographic Map from ESRI® (<http://www.arcgis.com/home/item.html?id=30e5fe3149c34df1ba922e6f5bbf808f>).

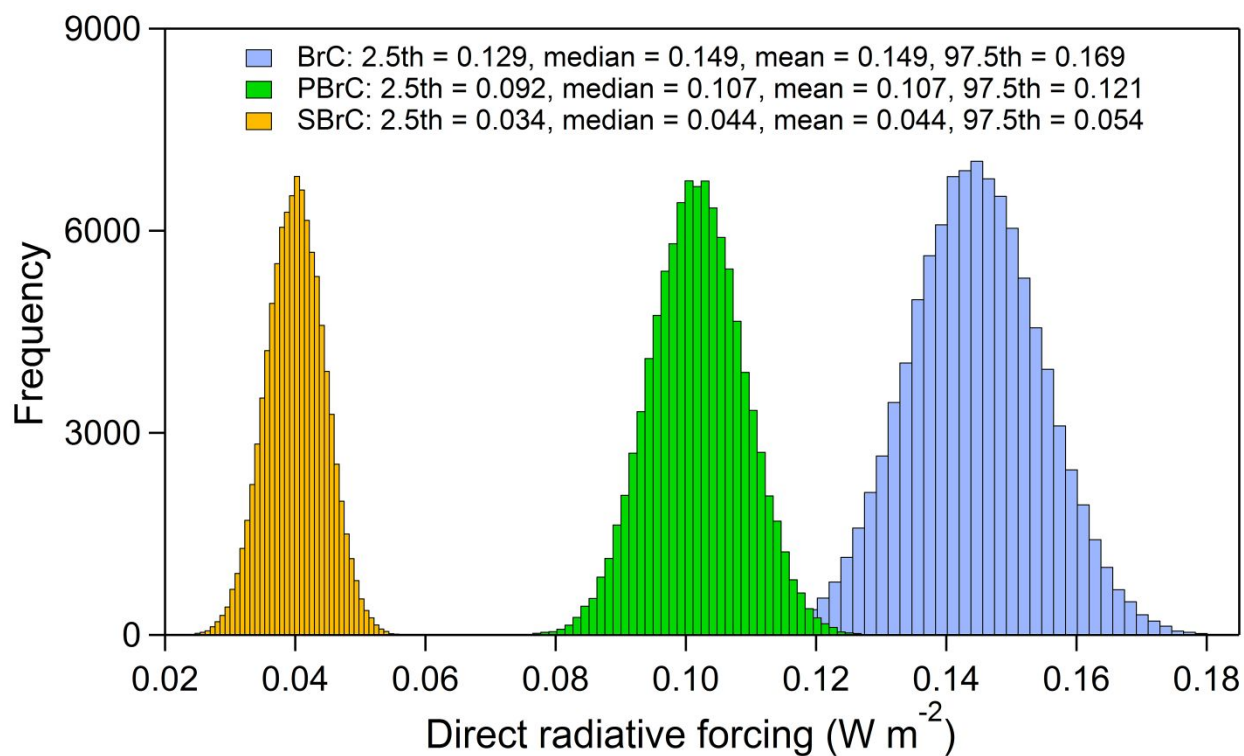


Figure S15. Probability distributions of direct radiative forcing for total brown carbon (BrC), primary BrC (PBrC), and secondary BrC (SBrC) based on 100,000 Monte Carlo simulations.

2.5th and 97.5th are percentiles.

References:

1. Collaud Coen, M.; Weingartner, E.; Apituley, A.; Ceburnis, D.; Fierz-Schmidhauser, R.; Flentje, H.; Henzing, J. S.; Jennings, S. G.; Moerman, M.; Petzold, A.; Schmid, O.; Baltensperger, U. Minimizing Light Absorption Measurement Artifacts of the Aethalometer: Evaluation of Five Correction Algorithms. *Atmos. Meas. Tech.* **2010**, *3* (2), 457–474.
2. Drinovec, L.; Močnik, G.; Zotter, P.; Prévôt, A. S. H.; Ruckstuhl, C.; Coz, E.; Rupakheti, M.; Sciare, J.; Müller, T.; Wiedensohler, A.; Hansen, A. D. A. The "dual-spot" Aethalometer: An Improved Measurement of Aerosol Black Carbon with Real-time Loading Compensation. *Atmos. Meas. Tech.* **2015**, *8* (5), 1965–1979.
3. Wang, Q.; Cao, J.; Han, Y.; Tian, J.; Zhu, C.; Zhang, Y.; Zhang, N.; Shen, Z.; Ni, H.; Zhao, S.; Wu, J. Sources and Physicochemical Characteristics of Black Carbon Aerosol from the Southeastern Tibetan Plateau: Internal Mixing Enhances Light Absorption. *Atmos. Chem. Phys.* **2018**, *18* (7), 4639–4656.
4. Tasoglou, A.; Saliba, G.; Subramanian, R.; Pandis, S. N. Absorption of Chemically Aged Biomass Burning Carbonaceous Aerosol. *J. Aerosol Sci.* **2017**, *113*, 141–152.
5. Qin, Y. M.; Tan, H. B.; Li, Y. J.; Li, Z. J.; Schurman, M. I.; Liu, L.; Wu, C.; Chan, C. K. Chemical Characteristics of Brown Carbon in Atmospheric Particles at a Suburban Site Near Guangzhou, China. *Atmos. Chem. Phys.* **2018**, *18* (22), 16409–16418.
6. Saleh, R.; Robinson, E. S.; Tkacik, D. S.; Ahern, A. T.; Liu, S.; Aiken, A. C.; Sullivan, R. C.; Presto, A. A.; Dubey, M. K.; Yokelson, R. J.; Donahue, N. M.; Robinson, A. L. Brownness of Organics in Aerosols from Biomass Burning Linked to Their Black carbon content. *Nat. Geosci.* **2014**, *7*, 647–650.
7. Kim, J.-H.; Kim, S.-W.; Ogren, J. A.; Sheridan, P. J.; Yoon, S.-C.; Sharma, S.; Lin, N.-H. Multiple Scattering Correction Factor Estimation for Aethalometer Aerosol Absorption Coefficient Measurement. *Aerosol Sci. Technol.* **2019**, *53*, (2), 160–171.
8. Paatero, P.; Hopke, P. K. Discarding or Downweighting High-noise Variables in Factor Analytic Models. *Anal. Chim. Acta* **2003**, *490* (1), 277–289.
9. Canonaco, F.; Crippa, M.; Slowik, J. G.; Baltensperger, U.; Prévôt, A. S. H. SoFi, An IGOR-based Interface for the Efficient Use of the Generalized Multilinear Engine (ME-2) for the Source Apportionment: ME-2 Application to Aerosol Mass Spectrometer Data. *Atmos. Meas. Tech.* **2013**, *6* (12), 3649–3661.
10. Elser, M.; Huang, R. J.; Wolf, R.; Slowik, J. G.; Wang, Q. Y.; Canonaco, F.; Li, G.; Bozzetti, C.; Daellenbach, K. R.; Huang, Y.; Zhang, R.; Li, Z.; Cao, J.; Baltensperger, U.; El-Haddad, I.; Prévôt, A. S. H. New Insights into PM_{2.5} Chemical Composition and Sources in Two Major Cities in China during Extreme Haze Events Using Aerosol Mass Spectrometry. *Atmos. Chem. Phys.* **2016**, *16* (5), 3207–3225.
11. Crippa, M.; Canonaco, F.; Lanz, V. A.; Äijälä, M.; Allan, J. D.; Carbone, S.; Capes, G.; Ceburnis, D.; Dall'Osto, M.; Day, D. A.; DeCarlo, P. F.; Ehn, M.; Eriksson, A.; Freney, E.; Hildebrandt Ruiz, L.; Hillamo, R.; Jimenez, J. L.; Junninen, H.; Kiendler-Scharr, A.; Kortelainen, A. M.; Kulmala, M.; Laaksonen, A.; Mensah, A. A.; Mohr, C.; Nemitz, E.; O'Dowd, C.; Ovadnevaite, J.; Pandis, S. N.; Petäjä, T.; Poulain, L.; Saarikoski, S.; Sellegri, K.; Swietlicki, E.; Tiitta, P.; Worsnop, D. R.; Baltensperger, U.; Prévôt, A. S. H. Organic Aerosol

Components Derived from 25 AMS Data Sets Across Europe Using a Consistent ME-2 Based Source Apportionment Approach. *Atmos. Chem. Phys.* **2014**, *14* (12), 6159–6176.

12. Paatero, P.; Tapper, U. Positive Matrix Factorization: A Non-negative Factor Model with Optimal Utilization of Error Estimates of Data Values. *Environmetrics* **1994**, *5* (2), 111–126.

13. Chow, J. C.; Watson, J. G.; Chen, L. W. A.; Chang, M. C. O.; Robinson, N. F.; Trimble, D.; Kohl, S. The IMPROVE_A Temperature Protocol for Thermal/Optical Carbon Analysis: Maintaining Consistency with a Long-Term Database. *J. Air Waste Manage. Assoc.* **2007**, *57* (9), 1014–1023.

14. Bond, T. C.; Bergstrom, R. W. Light Absorption by Carbonaceous Particles: An Investigative Review. *Aerosol Sci. Technol.* **2006**, *40* (1), 27–67.

15. Kondo, Y.; Sahu, L.; Kuwata, M.; Miyazaki, Y.; Takegawa, N.; Moteki, N.; Imaru, J.; Han, S.; Nakayama, T.; Oanh, N. T. K.; Hu, M.; Kim, Y. J.; Kita, K. Stabilization of the Mass Absorption Cross Section of Black Carbon for Filter-Based Absorption Photometry by the Use of a Heated Inlet. *Aerosol Sci. Technol.* **2009**, *43* (8), 741–756.

16. Yang, M.; Howell, S. G.; Zhuang, J.; Huebert, B. J. Attribution of Aerosol Light Absorption to Black Carbon, Brown Carbon, and Dust in China – Interpretations of Atmospheric Measurements during EAST-AIRE. *Atmos. Chem. Phys.* **2009**, *9* (6), 2035–2050.

17. Laskin, A.; Laskin, J.; Nizkorodov, S. A. Chemistry of Atmospheric Brown Carbon. *Chem. Rev.* **2015**, *115* (10), 4335–4382.

18. Shamjad, P. M.; Tripathi, S. N.; Pathak, R.; Hallquist, M.; Arola, A.; Bergin, M. H. Contribution of Brown Carbon to Direct Radiative Forcing over the Indo-Gangetic Plain. *Environ. Sci. Technol.* **2015**, *49* (17), 10474–10481.

19. Lack, D. A.; Langridge, J. M. On the Attribution of Black and Brown Carbon Light Absorption using the Ångström Exponent. *Atmos. Chem. Phys.* **2013**, *13* (20), 10535–10543.

20. Li, G.; Bei, N.; Tie, X.; Molina, L. T. Aerosol Effects on the Photochemistry in Mexico City during MCMA-2006/MILAGRO Campaign. *Atmos. Chem. Phys.* **2011**, *11* (11), 5169–5182.

21. Clegg, S. L.; Brimblecombe, P.; Wexler, A. S. Thermodynamic Model of the System $\text{H}^+ - \text{NH}_4^+ - \text{Na}^+ - \text{SO}_4^{2-} - \text{NO}_3^- - \text{Cl}^- - \text{H}_2\text{O}$ at 298.15 K. *J. Phys. Chem. A* **1998**, *102* (12), 2155–2171.

22. Friese, E.; Ebel, A. Temperature Dependent Thermodynamic Model of the System $\text{H}^+ - \text{NH}_4^+ - \text{Na}^+ - \text{SO}_4^{2-} - \text{NO}_3^- - \text{Cl}^- - \text{H}_2\text{O}$. *J. Phys. Chem. A* **2010**, *114* (43), 11595–11631.